RSC Advances

PAPER

View Article Online
View Journal | View Issue

Cite this: *RSC Adv.*, 2024, **14**, 32721

Development of a selective COX-2 inhibitor: from synthesis to enhanced efficacy *via* nano-formulation†

Marwa Elewa, ‡*[a] Mohamed Shehda,‡[b] Pierre A. Hanna, [c] Mohamed M. Said,[a] Sherif Ramadan, [de] Assem Barakat [f] and Yasmine M. Abdel Aziz *[a]

Non-steroidal anti-inflammatory drugs NSAIDs are widely used for managing various conditions including pain, inflammation, arthritis and many musculoskeletal disorders. NSAIDs exert their biological effects by inhibiting the cyclooxygenase (COX) enzyme, which has two main isoforms COX-1 and COX-2. The COX-2 isoform is believed to be directly related to inflammation. Based on structure–activity relationship (SAR) studies of known selective COX-2 inhibitors, our aim is to design and synthesize a novel series of 2-benzamido-*N*-(4-substituted phenyl)thiophene-3-carboxamide derivatives. These derivatives are intended to be selective COX-2 inhibitors through structural modification of diclofenac and celecoxib. The compound 2-benzamido-5-ethyl-*N*-(4-fluorophenyl)thiophene-3-carboxamide **VIIa** demonstrated selective COX-2 inhibition with an IC_{50} value of 0.29 μM and a selectivity index 67.24. This is compared to celecoxib, which has an IC_{50} value of 0.42 μM and a selectivity index 33.8. Molecular docking studies for compound **VIIa** displayed high binding affinity toward COX-2. Additionally, the suppression of protein denaturation with respect to albumin was performed as an indicative measure of the potential anti-inflammatory efficacy of the novel compounds. Compound **VIIa** showed potent anti-inflammatory activity with 93% inhibition and an IC_{50} value 0.54 μM. In comparison, celecoxib achieved 94% inhibition with an IC_{50} value 0.89 μM. Although molecule **VIIa** demonstrated significant *in vitro* anti-inflammatory activity, adhered to Lipinski's "five rules" (RO5) and exhibited promising drug-like properties, it showed indications of poor *in vivo* activity. This limitation is likely due to poor aqueous solubility, which impacts its bioavailability. This issue could be addressed by incorporating the drug in niosomal nanocarrier. Niosomes were prepared using the thin-film hydration technique. These niosomes exhibited a particle size of less than 200 nm, high entrapment efficiency, and an appropriate drug loading percentage. Transmission electron microscopy (TEM) and differential scanning calorimetry (DSC) studies revealed that the niosomes were spherical and demonstrated compatibility of all of its components. The drug release study indicated that the pure drug had limited practicality for *in vivo* use. However, incorporating the drug into niosomes significantly improved its release profile, making it more suitable for practical use.

Received 31st August 2024
Accepted 19th September 2024

DOI: 10.1039/d4ra06295g

rsc.li/rsc-advances

1. Introduction

Inflammation is a normal adaptive response to tissue injury, triggered by harmful stimuli such as physical trauma, microbial infections, allergens or noxious chemicals. It is associated with common disorders such as arthritis, asthma, *etc.*[1] The benefits of inflammation as an adaptive response include the destruction of invading organisms and the removal of irritants or foreign bodies, followed by the repair of injured tissue. The anti-inflammatory drugs exert their biological effects by inhibiting the cyclooxygenase COX enzyme, which has two main isoforms COX-1, and COX-2. COX-2 isoform is believed to be responsible for biosynthesis of prostaglandins PGs that are associated with inflammation. Non-steroidal anti-inflammatory drugs NSAIDs are among the most widely used drugs for the treatment of various inflammatory diseases and relieving pain.[2] Traditional

[a]*Pharmaceutical Organic Chemistry Department, Faculty of Pharmacy, Suez Canal University, Ismailia, Egypt. E-mail: marwa_elewa@pharm.suez.edu.eg; msaid123eg@yahoo.com; yasmine_abdelaziz@pharm.suez.edu.eg*

[b]*Department of Pharmaceutical Chemistry, Faculty of Pharmacy, Horus University-Egypt, New Damietta, Egypt. E-mail: Dr.shehda@gmail.com*

[c]*Department of Pharmaceutics and Industrial Pharmacy, Faculty of Pharmacy, Suez Canal University, Ismailia, 41522, Egypt. E-mail: pierre_hanna@pharm.suez.edu.eg*

[d]*Chemistry Department, Michigan State University, East Lansing, MI 48824, USA. E-mail: sramadan@chemistry.msu.edu*

[e]*Department of Chemistry, Benha University, Benha, Egypt*

[f]*Department of Chemistry, College of Science, King Saud University, P. O. Box 2455, Riyadh 11451, Saudi Arabia. E-mail: ambarakat@ksu.edu.sa*

† Electronic supplementary information (ESI) available. See DOI: https://doi.org/10.1039/d4ra06295g

‡ These authors contributed equally.

NSAIDs, such as diclofenac, exert their biological effects by inhibiting both COX-1 and COX-2 isoforms, making them non-selective COX inhibitors. Their non-selective inhibition on COX isoforms can lead to serious adverse effects.[3,4] It is worth noting that both COX-1 and COX-2 are highly similar in structure, sharing approximately 60–65% of their amino acid sequence, which makes them almost superimposable. COX isoforms have four domains, with the most crucial being the catalytic domain.[5] Although COX-1, and COX-2 isoforms are highly similar in structure, there is a notable structural difference in the active site (catalytic domain) of COX-2.[6,7] The COX-2 isoform has an active site that is approximately 20% larger than that of

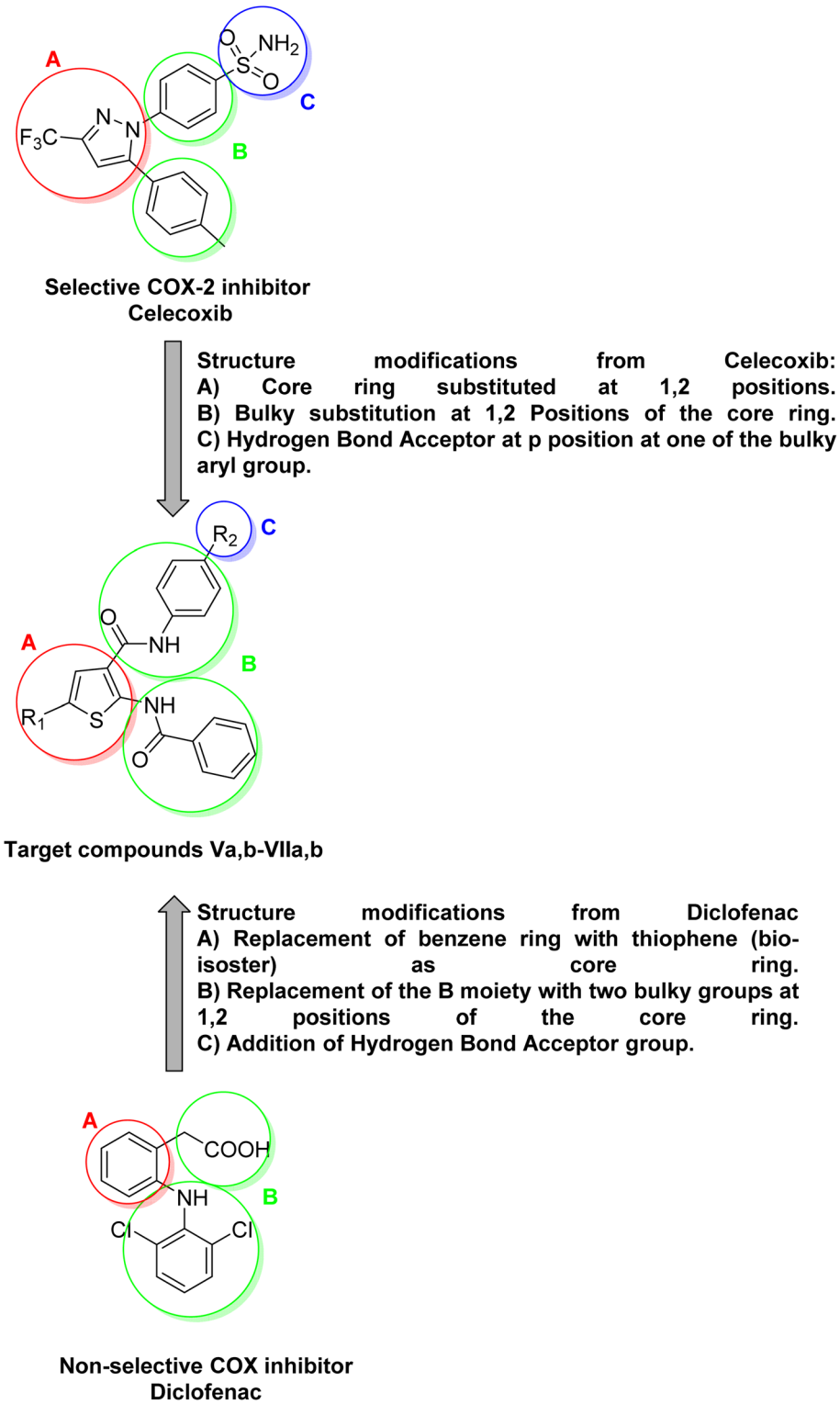

Fig. 1 The design of the target compounds.

COX-1 and also features a characteristic region for hydrogen bond formation.[8] Based on the structural differences between COX-1 and COX-2 isoforms, a variety of selective COX-2 inhibitors have been designed as anti-inflammatory agents. These inhibitors aim to minimize adverse effects associated with COX-1 inhibition.[9] The most well-known family of selective COX-2 inhibitors is the COXIBs. Structure–activity relationship (SAR) studies of celecoxib have identified three significant moieties. As shown in (Fig. 1), the first moiety is (A) a central ring substituted at the 1,2 positions. The second one is (B) bulky substitutions at the 1,2 positions of the central ring. The last moiety is (C) hydrogen bond acceptor substitution on the *para*-position of one of the two bulky aryl groups.[10] It is worth noting that, the structure of diclofenac lacks the characteristic hydrogen bond acceptor moiety (C) which is crucial for the selectivity towards COX-2. The aim of this research is to design and synthesize novel selective COX-2 inhibitors by modifying the structures of diclofenac and celecoxib as illustrated in (Fig. 1). The *in vitro* selectivity toward COX-2 compared to diclofenac and celecoxib as well as the drug-like properties of the novel compounds were investigated.

2. Results and discussion

2.1. Chemistry

Ethyl 2-aminothiophene-3-carboxylate derivatives **Ia**,**b** were obtained in a good yield following Gewald's aminothiophene reaction.[11,12] The synthesis of ethyl 2-benzamidothiophene-3-carboxylate derivatives **IIa**,**b** was achieved by the reaction of 2-aminothiophene derivatives **Ia**,**b** with benzoyl chloride in tetrahydrofuran (THF) in the presence of triethylamine (TEA).[13] The synthesis of 2-benzamidothiophene-3-carboxylic acid derivatives **IIIa**,**b** was achieved through a hydrolysis reaction. Ethyl 2-benzamidothiophene-3-carboxylate derivatives **IIa**,**b** was converted into their corresponding carboxylic acid derivatives by boiling the ester with sodium hydroxide and ethanol in basic hydrolysis reaction, followed by acidification with HCl.[14] The synthesis of 4*H*-thieno[2,3-*d*][1,3]oxazin-4-one derivatives **IVa**,**b** were achieved by refluxing 2-benzamidothiophene-3-carboxylic acid derivatives **IIIa**,**b** with acetic anhydride.[15] 2-Benzamido-*N*-phenylthiophene-3-carboxamide derivatives **Va**,**b**–**VIIa**,**b** were obtained by condensation reaction between 4*H*-thieno[2,3-*d*][1,3]oxazin-4-one derivatives **IVa**,**b** and *p*-substituted aniline in glacial acetic acid (AcOH) (Scheme 1).[15]

The structures of these newly synthesized compounds **Va**,**b**–**VIIa**,**b** were confirmed by spectral data (IR spectroscopy, ^{1}H-NMR, ^{13}C-NMR, mass spectroscopy). The IR spectra showed two broad peaks around 3400 and 3350 cm^{-1}, corresponding to the secondary amine groups of the amides. Additionally, two peaks around 1610 and 1530 cm^{-1}, were observed, representing the carbonyl groups of the amides. The ^{1}H-NMR spectra of these compounds revealed two singlets around 12.5 ppm and 10 ppm representing the two exchangeable protons of the two amides. The aromatic region displayed several signals integrating to 10 protons, corresponding to the two benzene rings and the proton of thiophene ring. The aliphatic region showed the characteristic signals for the ethyl and propyl groups in series a and b, respectively. The ^{13}C-NMR spectra showed two signals for the

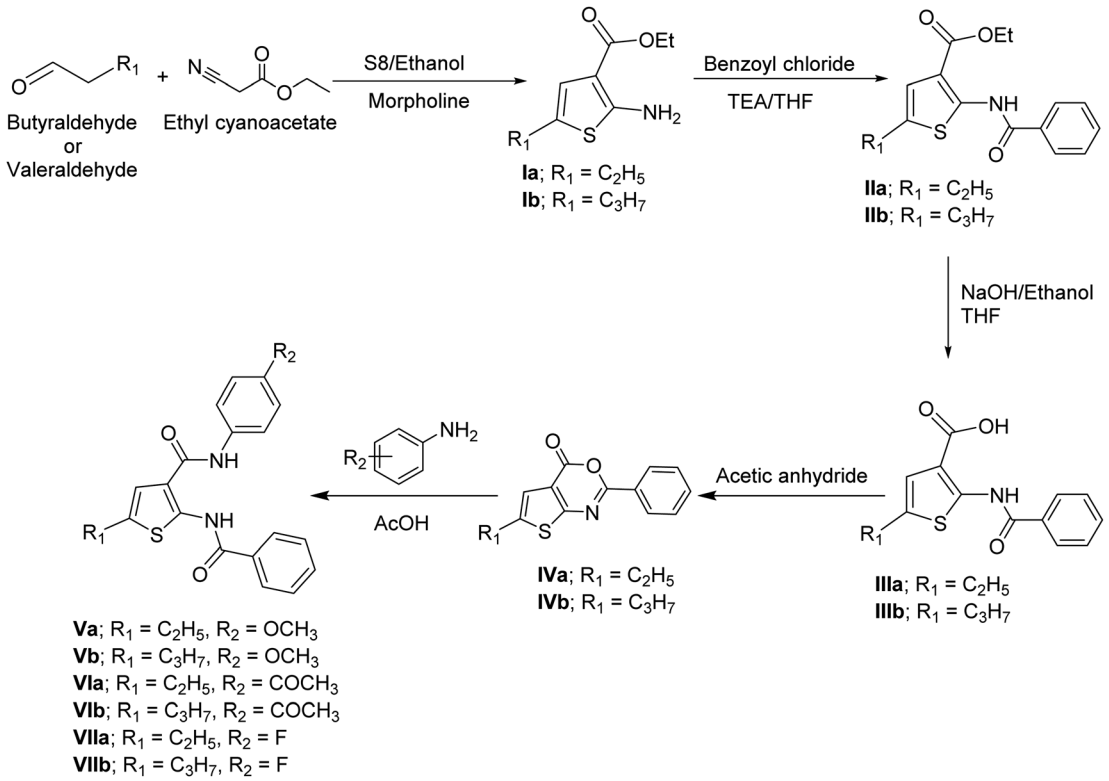

Scheme 1 Synthesis of thiophene-3-carboxamide derivatives.

two carbons of the two carbonyl groups at 165 ppm and 160 ppm. The aromatic region showed number of signals corresponding to their aromatic rings. The aliphatic region showed the characteristic signals for the ethyl and propyl groups in series a and b, respectively.

2.2. Biological activity

2.2.1. Cyclooxygenase inhibition assays. Tested compounds were screened against COX-1 and COX-2 inhibitory activities along with the calculation of selectivity index as summarized in (Table 1). The results showed that all compounds exhibited potent selective COX-2 inhibition with IC_{50} values ranging from 0.29–3.3 μM. In contrast, COX-1 inhibition was less potent, with IC_{50} values ranging from 15.7 to 26.6 μM. Interestingly, compound 2-benzamido-5-ethyl-*N*-(4-fluorophenyl) thiophene-3-carboxamide **VIIa** showed potent and selective COX-2 inhibition with an IC_{50} value of 0.29 μM and an a selectivity index (SI) of 67.2. This compares favorably to celecoxib, which has an IC_{50} value of 0.42 μM and an SI of 33.8, and to diclofenac sodium, which has an SI of 1.80.

2.2.2. The *in vitro* anti-inflammatory assay using egg albumin. An indicator of the anti-inflammatory efficacy was the suppression of protein denaturation, specifically with respect to albumin. As seen in (Table 2), compound **VIIa** showed potent anti-inflammatory activity having 93% inhibition at the higher concentration with an IC_{50} value 0.54 μM compared to celecoxib that has had 94% inhibition with IC_{50} 0.89 μM. Additionally, compounds **VIIb**, **Va**, **VIb** and **VIa** showed promising anti-inflammatory activities with an IC_{50} values of 1.13, 1.9, 1.94, and 1.34 μM showing inhibition percentages of 86, 85, 85, and 81%, respectively. While compound **Vb** showed moderate activity with IC_{50} values 3.29 μM and with inhibition percentages of 78%. The findings from the *in vitro* cyclooxygenase inhibition experiment are consistent with these observations.

2.3. *In silico* studies

2.3.1. Molecular docking. Molecular docking study was conducted to highlight the binding affinity of the tested compound **VIIa** towards the binding sites of both COX-1, and COX-2 proteins. As summarized in (Table 3), celecoxib formed three H-bond interactions with Ser 353, His 90 and Gln 192 inside COX-1 protein, while it formed two H-bond with Ser 530 and Arg 120 inside the COX-2 protein. So, in comparison with celecoxib, compound **VIIa** exhibited promising binding affinity towards COX-2 protein with binding energy of -14.25 kcal mol^{-1}, and it formed one H-bond interaction with Ser 530 and van der Waals force with Arg 120 (Fig. 2B). While, it was docked inside COX-1 protein forming unstable drug–protein complex (positive binding energy), and it shows no interactions with the key amino acids inside COX-1 protein (Fig. 2A). Hence compound **VIIa** showed selective COX-2 inhibition and this completely agreed with the experimental results.

Table 1 COX-1 and COX-2 inhibitory activities with IC_{50} and selective index values

	IC_{50} μM [a]		
Compound	COX-1	COX-2	Selectivity index (SI)[b]
Va	24.3	1.98	12.27
Vb	26.6	3.35	7.94
VIa	21.3	0.86	24.76
VIb	15.7	1.23	12.75
VIIa	19.5	0.29	67.24
VIIb	16.6	0.85	19.52
Diclofenac	0.09	0.05	1.8
Celecoxib	14.2	0.42	33.80

[a] IC_{50} values are calculated as the concentration that make 50% inhibition of COX-1 or COX-2. [b] Selectivity index (SI) = IC_{50} (COX_1)/IC_{50} (COX_2).

Table 2 IC_{50} values for protein denaturation inhibition and percentage of inhibition

Compound	IC_{50} of inhibition	% inhibition at the higher concentration
Va	1.9	85%
Vb	3.29	78%
VIa	1.34	81%
VIb	1.95	85%
VIIa	0.54	93%
VIIb	1.13	86%
Celecoxib	0.89	94%

2.3.2. Bioinformatics study. The drug-likeness score and physicochemical characteristics of **VIIa**, which exhibited the highest selective COX-2 activity, were predicted using ADME pharmacokinetics (SwissADME® Software). Based on ADME study, compound **VIIa** had a molecular weight of 368.4*D*, volume of 318.6A^3, polar surface area of 58.2A^2, log *P* (octanol–water partition coefficient) value of 3.08, 3 H-bond acceptors and 2 H-bond donors. Fig. 3A shows that using the "Boiled Egg" model, the drug appeared in the egg white but not the egg yolk. This indicated that the drug could not pass through the blood-brain barrier, however, it can be passively absorbed through the gastrointestinal tract.

Some of the predicted physicochemical and pharmacokinetic properties of the drug are listed in Table 4. According to these values, the drug aqueous solubility was shown to be 7.02 $\times$ 10^{-6} mg mL^{-1} This indicated that the drug is under the category of poorly water soluble. The gastrointestinal absorption of this drug was predicted to be high. Combining both physicochemical and pharmacokinetic parameters suggests that the drug could be categorized as class II based on biopharmaceutical classification system (BCS).

Hence molecular properties of compound **VIIa** obeyed Lipinski's "five rules" (RO5) and exhibited promising drug-like properties as illustrated in (Fig. 3B). Lipophilicity of compound **VIIa** was shown by Fig. 3C to be high. This might be participating to the poor aqueous solubility of the compound and high log $P_{o/w}$ value.

As a result of these studies, the compound **VIIa** is suggested to be considered as a "drug candidate" that is an efficient anti-inflammatory with selective COX-1 inhibition effect. According

Table 3 Summary of ligand–receptor interactions of the docked compound **VIIa** compared to celecoxib as standard drug

Ligands	Protein	Binding energy (kcal mol^{-1})	Number of H-bonds	Active site residues	Bonds length (Å)
Celecoxib	COX-1	−7.9	3	Ser 353	1.96
				His 90	2.01
				Gln 192	2.03
	COX-2	−7.50	2	Ser 530	1.16
				Arg 120	1.23
VIIa	COX-1	1.26	—	—	—
	COX-2	−14.25	1	Ser 530	1.66
				van der Waals interactions Arg 120	

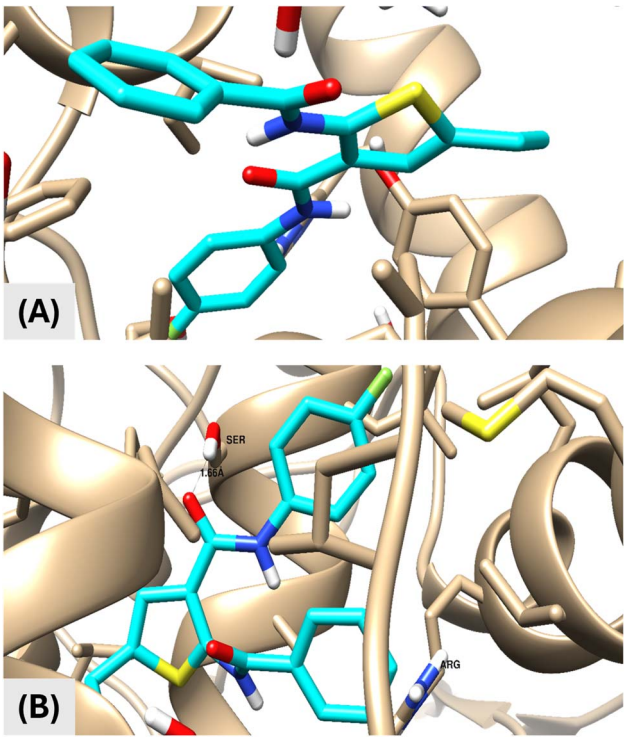

Fig. 2 Binding disposition and interactive mode of the docked compound **VIIa** (cyan-colored) towards COX-1 (A) and COX-2 (B). Three-dimensional images were generated by Chimera-UCSF. Docking calculation was carried out using AutoDock Vina and visualization was made by Chimera-UCSF software.

to BCS, the drug is classified as a class II member due to its poor solubility with high GI permeability.

2.4. Development of niosomal formulation to enhance drug efficacy

As stated earlier the drug candidate was predicted to belong to BCS class II. This indicates that the aqueous solubility of this candidate could be a great obstacle facing the delivery of the drug and its practical use. Since the lipophilicity of the drug was shown to be high, a lipid-based nano drug delivery system was shown to be the drug delivery system of choice. Niosomes were chosen to be the nanoparticulate drug delivery system for the delivery of this drug candidate. They are analogous to liposomes in that they could be prepared following the same procedures, under a variety of conditions, leading to the formation of unilamellar or multilamellar vesicular structures.[16] When compared to phospholipid-based vesicles, the surfactant vesicles have several advantages such as greater stability, thus lesser care in handling and storage and lower cost. These advantages make surfactant vesicles more attractive than phospholipid ones for industrial applications both in the field of pharmaceutics and cosmetics.[17–19] The aim of this section was to improve the delivery of the drug and enhance its dissolution and release characteristics to enhance the practical utility of the drug so that it can be transferred to *in vivo* studies and clinical phases of the study.

2.4.1. Quantification of the drug using UV spectrophotometry. Spectrophotometric techniques measure solute

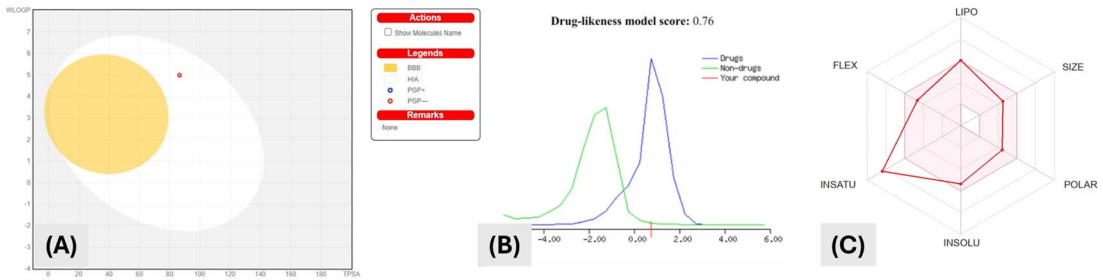

Fig. 3 (A) BOILED-Egg model for compound **VIIa** using SwissADME. (B) Drug likeness score of compound **VIIa** using MolSoft "The green region indicates that the behavior is not drug-like, whereas the blue area indicates that it is drug-like". (C) Radar for predicted bioavailability where colored zone represent good oral bioavailability (SwissADME®).

Table 4 Predicted physicochemical properties and pharmacokinetics behavior of the drug

Physicochemical properties		Pharmacokinetic behavior	
Molecular weight	368.42 g mol^{-1}	GI absorption	High
Log $P_{o/w}$	3.08	BBB penetration	No
Aqueous solubility at 25 °C	7.02×10^{-6} mg mL	Log K_p (skin permeation)	-4.93 cm s^{-1}

concentration in a solution by assessing the light absorbed by the solution. A spectrophotometer directs light through the solution and measures the intensity of the light that emerges, leveraging the dual nature of light for this analysis. In spectrophotometric techniques, the goal is often to analyze the drug of interest within a matrix that includes excipients, additives, degradation products, impurities, and, in the case of combination products, other drugs.[20]

The main advantages of using spectrophotometric techniques for determination of drug concentrations in the solutions are the low cost, simplicity and less time consumption.[21]

Regarding the alcoholic solution of the drug in study, two absorbance peaks (λ_{max}) were manifested. One appeared at 272 nm while the other appeared at 334 nm. Both peaks showed absorbances that were strongly positively correlated to the concentration of the drug all over the range of concentration used for construction of the calibration curve. However, the peak appearing at 334 was chosen to be the one used for quantification of the drug because of higher regression value for the whole concentration range detected. Calibration curves of the drug in ethanol for both peaks were shown by (Fig. 4A). The absorbance of the drug in ethanol was shown to be following Beer's–Lambert's law within the whole range of concentrations used in the experiment. Linearity range was shown to be from 2.5–25 μg mL^{-1}. The regression coefficient (R^2) value was calculated and shown to be 0.9995 suggesting very strong correlation between concentration and absorbance and hence good accuracy and reproducibility.

Calibration curve of the drug in aqueous solution at pH 6.8 was illustrated not to differ so much from ethanol. The absorbance peak was shifted from 334 nm to become 346 nm. This is suggested to take place due to protonation of some active centers in the molecule. Also, the regression was also reliable, yet, it was reduced as compared to that of the drug in ethanol. Calibration curve of the drug at pH 6.8 is illustrated by (Fig. 4B).

2.4.2. Physicochemical characterization of the prepared niosomal dispersion. Niosomal formulations were characterized for their physicochemical characteristics to determine their suitability as a nanocarrier system to improve efficacy of the newly synthesized new chemical entity. Physicochemical characterizations included measurement of yield percentage, particle size, particle size distribution (span), entrapment efficiency, and percentage drug loading. Values of these characteristics of the plain niosomal nanocarrier system (PNi) and drug-loaded one (DNi) are listed in (Table 5).

As shown by (Table 5), yield percentage values of both formulae exceeded 85%. This could be generally considered to be an efficient system for industrial scale up. The yield of PNi was shown to be slightly, yet significantly, higher than that of the DNi system. This was reported in many nanocarrier systems.[22] This was suggested to take place as a result of the infusion of some of the drug to the medium resulting in reduction in the final overall weight of the formulated particles.[23]

It was clearly demonstrated, regarding particle size and particle size distribution, expressed as span value, that both PNi and DNi formulations were of appropriate particle size range and distribution. Particles of size below 150 nm manifested extraordinary characteristic including increasing solubility and penetration of drugs.[24] Both PNi and DNi showed particle sizes

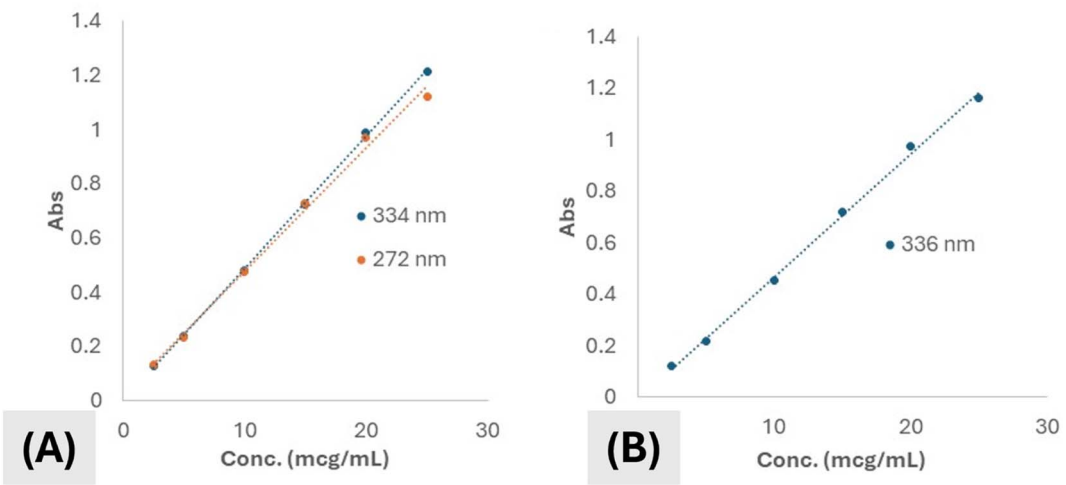

Fig. 4 Calibration curves of (A) drug in ethanol and (B) drug in buffered solution, pH 6.8.

Table 5 Physicochemical characteristics of the prepared niosomal formulations

	Yield (%)	Particle size (nm)	Span	Entrapment efficiency	Drug loading (%)
PNi	88.41% ± 3.04	107.33 ± 1.15	1.08 ± 0.06	—	—
DNi	85.73% ± 2.97	116.00 ± 3.6	1.12 ± 0.13	78.28% ± 3.01	23.81% ± 2.74

below 150 nm and span values indicating almost a single particles population with narrow distribution. Nevertheless, incorporating the drug in nanoparticles resulted in mild increase in the particles size, however, the changed particles size remained below 150 nm, indicating no major change in the enhancing solubility capabilities of the nanosystem.[24]

Particles showed a good entrapment of the drug. The value of percentage drug entrapped within the particles was suggested to be high due of two reasons; the first is the technique used and the second one is that the drug was of high solubility in the base used and low solubility in the external phase (aqueous phase).[25] The drug loading of DNi suggested that the particles could be properly used for delivering the drug at its therapeutics dose without the use of much weight of the formula.

2.4.3. Determination of thermal behavior of the drug and possible physical intteractions. It was shown from thermal analysis of the drug that there was a tiny endothermic peak at 152 °C. This peak indicated the process of melting. The DSC thermogram of the pure drug is shown in (Fig. 5).

By comparing the DSC thermograms of the pure drug, PNi formula, and DNi niosomes, it was clearly evidenced that the drug was totally dispersed at molecular level in niosomes. This is indicated through the absence of the endothermic peak of the pure drug in the drug-loaded nanoparticles thermogram.[23] This was clearly illustrated by (Fig. 5).

2.4.4. Transmission electron microscopy (TEM). Inspection of morphological characteristics of the DNi formulation showed that the nanoparticles were completely spherical with

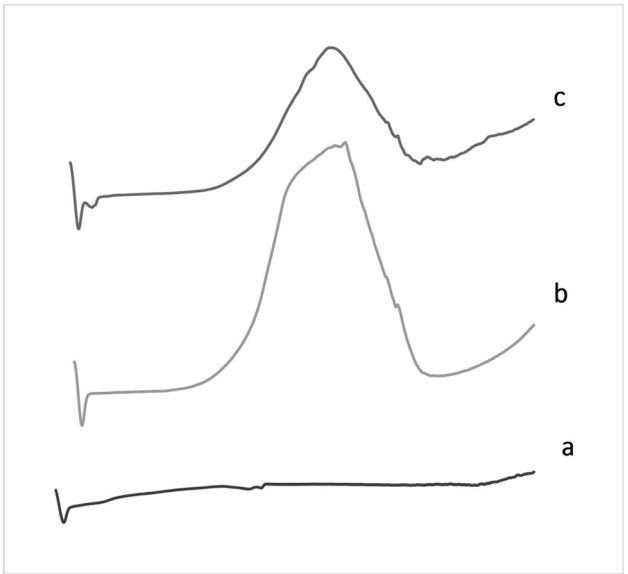

Fig. 5 DSC Thermograms of (a) pure drug, (b) PNi, and (c) DNi.

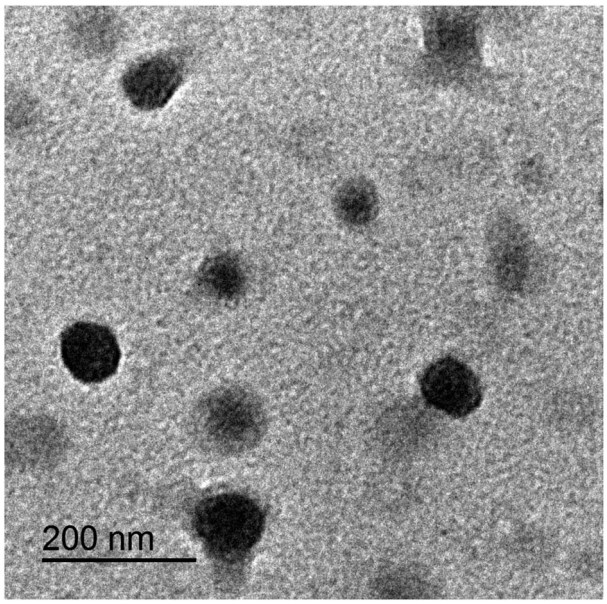

Fig. 6 Transmission electron micrograph of DNi formulation.

the prominent appearance of the bilayer of the nonionic surfactants membrane. This was demonstrated by (Fig. 6).

2.4.5. *In vitro* drug release profile. As illustrated by (Fig. 7), it was clearly evidenced that formulation of the drug candidate in a niosomal formulation affected enormously the pattern of the drug release. Being poorly water-soluble drug candidate, the drug in study manifested a release percentage of no more than 35% after 12 hours. On the other hand, the same drug candidate in the same dose showed a release percentage of about 85% after 12 hours. This could be justified on the basis of the

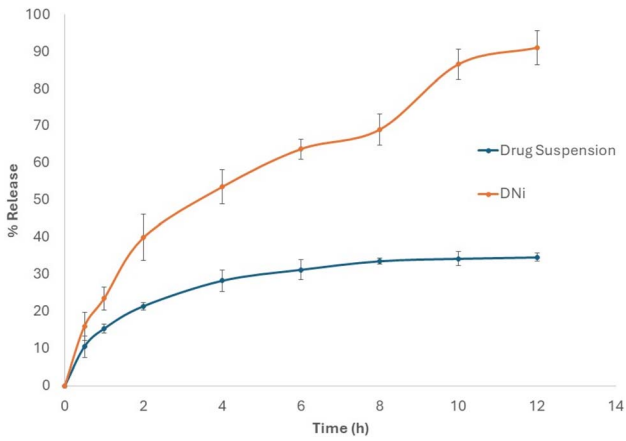

Fig. 7 Release pattern of the drug candidate for drug suspension and DNi formulation.

capability of the niosomal nanocarriers to increase drugs aqueous solubility.[26]

The solubility of a drug can significantly impact its bioavailability, absorption rate, and ultimately, its effectiveness as a therapeutic agent. This illustrates the importance of incorporating the drug candidate in a niosomal nanocarrier in order to enhance solubility, improve release pattern and finally improve bioavailability.[26,27]

2.4.6. Limitations and further work. Limitations of this study could be summarized in the lack of safety as well as dose–response curve evaluation. *In vivo* studies on animals are important to transfer the drug from preclinical phases of the study to the clinical ones. *In vivo* studies evaluating the dose–response correlation of this drug candidate, safety, and therapeutic range for this drug will be conducted in further research work. Additionally, the effect of formulating the drug on the *in vivo* pharmacokinetic behavior of the drug will be evaluated. Finally, incorporating the niosomal formulation containing the drug candidate in a fast dissolving film will be done to obtain a fast onset of action. The formula of this film will be optimized and the characteristics of this film will also be evaluated.

3. Materials and methods

3.1. Chemistry

"Stuart melting point apparatus SMP10 was used for melting points determination. Melting points were uncorrected. Vector 22 infrared spectrophotometer (υ_{max} in cm^{-1}) was used to measure infrared (IR) spectra. Nuclear magnetic resonance ^1H NMR spectra were recorded on Bruker spectrometer (400–500 MHz). ^{13}C NMR spectra were carried out at either 100 or 125 MHz. Chemical shifts (δ) are indicated in ppm. Electron impact mass spectra (EI-MS) were recorded on a Finnigan MAT 312 mass spectrometer.

3.1.1. Synthesis of ethyl 2-aminothiophene-3-carboxylate derivatives Ia,b. Butyraldehyde or valeraldehyde (0.28–0.34 gram, 3.96 mmol) and ethyl cyano acetate (0.45 gram, 3.96 mmol) were dissolved in 70% ethanol (50 mL). Sulfur (127 mg, 3.96 mmol) was added to the reaction mixture portion-wise. The reaction mixture was stirred at 45 °C for 10 min. Morpholine (1.6 mL, 5.54 mmol) was added dropwise over 20 min. The reaction mixture was then stirred for additional 24 h at 60 °C. The completion of reaction was monitored using TLC. The mixture was poured on crushed ice forming yellow crystals. The resulting crystals were washed with cold water, dried and recrystallized from 95% ethanol.[28] Compound **Ia** yellow powder; yield 89%; m.p.: 70–72 °C as reported.[29] Compound **Ib** brownish-yellow solid; yield 81%; m.p.: 40–42 °C as reported.[30]

3.1.2. Synthesis of ethyl 2-benzamidothiophene-3-carboxylate derivatives IIa,b. Benzoyl chloride (0.89 gram, 6.4 mmol) was added to a stirred solution of ethyl 2-aminothiophene-3-carboxylate derivatives (**Ia,b**) (1.15–1.23 gram, 5.8 mmol) in THF (150 mL). Then TEA (12 mL) was added dropwise. After 6–12 h at RT, the completion of reaction was monitored using TLC then the mixture was filtered and the filtrate was concentrated, and recrystallized from 95% ethanol.[13] Compound **IIa** grayish white crystals; yield 82%; m.p.: 83–84 °C as reported.[31] Compound **IIb** brownish powder; yield 79%; mp 78–80 °C as reported.[32]

3.1.3. Synthesis of 2-benzamidothiophene-3-carboxylic acid derivatives IIIa,b. A solution of sodium hydroxide (1.83 g) in water (20 mL) was added to a stirred solution of ethyl 2-benzamidothiophene-3-carboxylate derivatives (**IIa,b**) (0.79–0.85 gram, 4.62 mmol) in THF (20 mL), with addition of 95% ethanol (20 mL). After 24 h at 75 °C, the completion of reaction was monitored using TLC, and water (100 mL) was added, then 2 N HCl was added until pH = 6. The precipitate is filtered and washed with water (3 × 10 mL) to afford the solid compound.[33]

Compound **IIIa**: white powder; yield 92%; m.p.: 201–202 °C as reported.[34]

Compound **IIIb**: reddish white powder; yield 90%; m.p.: 162–164 °C. ^1H NMR (400 MHz, DMSO-d_6) δ 12.96 (s, 1H, OH), 11.75 (s, 1H, NH), 7.68–7.66 (d, J = 7.3 Hz, 2H), 7.45–7.35 (m, 3H), 6.68 (s, 1H), 2.46–2.43 (t, J = 7.3 Hz, 2H), 1.40–1.35 (m, 2H), 0.70–0.66 (t, J = 7.3 Hz, 3H). ^{13}C NMR (100 MHz, DMSO-d_6) δ 167.20, 163.01, 146.41, 135.04, 133.28, 132.41, 129.70, 127.52, 121.26, 113.98, 31.13, 24.52, 13.85.

3.1.4. Synthesis of 4*H*-thieno[2,3-*d*][1,3]oxazin-4-one derivatives IVa, IVb. A solution of 2-benzamidothiophene-3-carboxylic acid derivatives **IIIa,b** (2 g) in acetic anhydride (10 mL) was stirred for 1 h at 140 °C. The completion of reaction was monitored using TLC. After the completion of the reaction solvent was nearly evaporated under reduced vacuum, then glacial acetic acid from the next step was added and used in the next reaction without separation.[33,34]

3.1.5. Synthesis of 2-benzamido-*N*-phenylthiophene-3-carboxamide derivatives Va,b–VIIa,b. A solution of 4*H*-thieno[2,3-*d*][1,3]oxazin-4-one derivatives **IVa,b** (1.28/1.32 gram, 5 mmol) in glacial acetic acid (10 mL) was stirred with aniline derivatives (5 mmol) and heated at reflux for 24 h. After cooling, the reaction mixture was poured on ice-water portion wise while stirring and the separated solid was filtered, dried and recrystallized from 95% ethanol.[33]

3.1.6. 2-Benzamido-5-ethyl-*N*-(4-methoxyphenyl) thiophene-3-carboxamide Va. Gray powder; yield 85%; m.p.: 168–169 °C; IR (KBr, cm^{-1}): 3392, 3348, 3055, 2966, 2925, 1653, 1626, 1564; ^1H-NMR (500 MHz, DMSO-d_6): δ = 13.08 (s, 1H, NH), 9.92 (s, 1H, NH), 7.93–7.91 (d, J = 7.3 Hz, 2H), 7.69–7.60 (m, 5H), 7.49 (s, 1H), 6.96–6.94 (d, J = 8.6 Hz, 2H), 3.75 (s, 3H), 2.81–2.76 (q, J = 7.3 Hz, 2H), 1.31–1.28 (t, J = 7.4 Hz, 3H); ^{13}C-NMR (125 MHz, DMSO-d_6): δ = 163.81, 162.29, 156.04, 144.49, 136.22, 132.74, 132.05, 130.93, 129.28, 126.99, 123.26, 118.63, 115.17, 113.79, 55.23, 22.32, 15.45; MS (m/z): 380.40 $[M]^+$; anal. for $C_{21}H_{20}N_2O_3S$: calc. C, 66.30; H, 5.30; N, 7.36; O, 12.62; S, 8.43, found: C, 66.32; H, 5.31; N, 7.35; O, 12.61; S, 8.42.

3.1.7. 2-Benzamido-*N*-(4-methoxyphenyl)-5-propyl thiophene-3-carboxamide Vb. Brown powder; yield 75%; m.p.: above 300 °C; IR (KBr, cm^{-1}): 3569, 3422, 3086, 2957, 2924, 1660, 1602, 1562; ^1H-NMR (400 MHz, DMSO-d_6): δ = 13.07 (s, 1H, NH), 9.89 (s, 1H, NH), 7.92–7.90 (d, J = 7.1 Hz, 2H), 7.69–7.58 (m, 5H), 7.46 (s, 1H), 6.96–6.93 (d, J = 8.9 Hz, 2H), 3.74 (s, 3H), 2.75–2.71 (t, J = 7.2 Hz, 2H), 1.70–1.65 (hextet, J = 7.2 Hz, 2H), 0.98–0.94 (t, J = 7.2 Hz, 3H); ^{13}C-NMR (100 MHz, DMSO-d_6): δ = 168.63, 164.28, 156.54, 145.07, 134.89, 133.97, 133.20,

132.56, 129.75, 127.47, 123.73, 119.89, 117.83, 114.28, 55.68, 31.39, 24.54, 13.95; MS (*m*/*z*): 394.60 $[M]^+$; anal. for $C_{22}H_{22}N_2O_3S$: calc. C, 66.98; H, 5.62; N, 7.10; O, 12.17; S, 8.13, found: C, 66.99; H, 5.64; N, 7.09; O, 12.16; S, 8.12.

3.1.8. *N*-(4-Acetylphenyl)-2-benzamido-5-ethyl thiophene-3-carboxamide *via*. Brown powder; yield 82%; m.p.: 225–227 °C; IR (KBr, cm^{-1}): 3453, 3346, 3020, 2958, 2928, 1649, 1599, 1521; ^{1}H-NMR (500 MHz, DMSO-d_6): δ = 12.83 (s, 1H, NH), 10.21 (s, 1H, NH), 8.00–7.98 (d, J = 8.7 Hz, 2H), 7.94–7.91 (m, 4H), 7.70–7.67 (t, J = 7.2 Hz, 1H), 7.65–7.62 (t, J = 7.4 Hz, 2H), 7.52 (s, 1H), 2.82–2.78 (q, J = 7.5 Hz, 2H), 2.55 (s, 3H), 1.31–1.28 (t, J = 7.4 Hz, 3H); ^{13}C-NMR (125 MHz, DMSO-d_6): δ = 196.72, 164.27, 162.54, 145.55, 142.79, 136.36, 132.86, 132.35, 132.00, 129.33, 129.28, 127.08, 120.31, 118.68, 114.98, 26.55, 22.32, 15.47; MS (*m*/*z*): 392.96 $[M]^+$; anal. for $C_{22}H_{20}N_2O_3S$: calc. C, 67.33; H, 5.14; N, 7.14; O, 12.23; S, 8.17, found: C, 67.32; H, 5.15; N, 7.13; O, 12.25; S, 8.16.

3.1.9. *N*-(4-Acetylphenyl)-2-benzamido-5-propylthiophene-3-carboxamide VIb. Yellowish green powder; yield 71%; m.p.: above 300 °C; IR (KBr, cm^{-1}): 3449, 3367, 3057, 2958, 2924, 1657, 1583, 1494; ^{1}H-NMR (400 MHz, DMSO-d_6): δ = 13.75 (s, 1H, NH), 11.35 (s, 1H, NH), 8.07–8.05 (d, J = 6.9 Hz, 2H), 7.95–7.93 (d, J = 8.4 Hz, 2H), 7.83–7.81 (d, J = 8.4 Hz, 2H), 7.48–7.41 (m, 3H), 6.86 (s, 1H), 2.59–2.56 (t, J = 7.2 Hz, 2H), 2.52 (s, 3H), 1.64–1.55 (hextet, J = 7.2 Hz, 2H), 0.93–0.90 (t, J = 7.2 Hz, 3H); ^{13}C-NMR (100 MHz, DMSO-d_6): δ = 196.76, 164.06, 158.47, 145.49, 140.95, 136.01, 130.85, 130.31, 129.79, 129.71, 128.29, 128.01, 120.64, 118.19, 116.51, 32.31, 26.83, 24.60, 14.06; MS (*m*/*z*): 406.67 $[M]^+$; anal. for $C_{23}H_{22}N_2O_3S$: calc. C, 67.96; H, 5.46; N, 6.89; O, 11.81; S, 7.89, found: C, 67.97; H, 5.45; N, 6.88; O, 11.83; S, 7.88.

3.1.10. 2-Benzamido-5-ethyl-*N*-(4-fluorophenyl) thiophene-3-carboxamide VIIa. Brown powder; yield 89%; m.p.: 162–163 °C; IR (KBr, cm^{-1}): 3440, 3372, 3084, 2966, 2926, 1634, 1562, 1506; ^{1}H-NMR (400 MHz, DMSO-d_6): δ = 12.97 (s, 1H, NH), 10.04 (s, 1H, NH), 7.95–7.93 (d, J = 7.2 Hz, 2H), 7.77–7.74 (dd, J = 8.8, 5.1 Hz, 2H), 7.71–7.62 (m, 3H), 7.49 (s, 1H), 7.26–7.22 (t, J = 8.8 Hz, 2H), 2.83–2.78 (q, J = 7.4 Hz, 2H), 1.33–1.29 (t, J = 7.5 Hz, 3H); ^{13}C-NMR (100 MHz, DMSO-d_6): δ = 164.45, 162.84, 160.39, 145.37, 136.77, 134.91, 133.23, 132.49, 129.75, 127.48, 123.94, 119.05, 115.85, 115.45, 22.78, 15.91; MS (*m*/*z*): 368.56 $[M]^+$; anal. for $C_{20}H_{17}FN_2O_2S$: calc. C, 65.20; H, 4.65; F, 5.16; N, 7.60; O, 8.69; S, 8.70, found: C, 65.22; H, 4.67; F, 5.15; N, 7.59; O, 8.68; S, 8.69.

3.1.11. 2-Benzamido-*N*-(4-fluorophenyl)-5-propyl thiophene-3-carboxamide VIIb. Yellowish green powder; yield 77%; m.p.: above 300 °C; IR (KBr, cm^{-1}): 3444, 3336, 3049, 2960, 2928, 1640, 1560, 1491; ^{1}H-NMR (400 MHz, DMSO-d_6) δ = 12.94 (s, 1H, NH), 10.04 (s, 1H, NH), 8.05 (d, J = 7.2 Hz, 2H), 7.72 (d, J = 8.8 Hz, 2H), 7.42–7.41 (m, 3H), 7.18–7.16 (d, J = 8.8 Hz, 2H), 6.87 (s, 1H), 2.68–2.64 (t, 7.2 Hz, 2H), 1.67–1.60 (m, 2H), 0.94–0.85 (t, J = 7.5 Hz, 3H); ^{13}C-NMR (100 MHz, DMSO-d_6): δ = 167.38, 163.88, 158.91, 157.48, 143.97, 141.07, 137.42, 135.01, 129.49, 127.94, 123.93, 120.80, 116.73, 115.91, 32.34, 24.62, 14.02; MS (*m*/*z*): 382.35 $[M]^+$; anal. for $C_{21}H_{19}FN_2O_2S$: calc. C, 65.95; H, 5.01; F, 4.97; N, 7.32; O, 8.37; S, 8.38, found: C, 65.98; H, 5.02; F, 4.96; N, 7.31; O, 8.36; S, 8.37.

3.2. Biological evaluation

The experimental protocols were approved by the Ethics Committee of the Suez Canal University with code 201802M1. We would like to confirm that our study does not involve any experiments with live subjects; all experiments were conducted *in vitro*, not *in vivo*.

3.2.1. Cyclooxygenase inhibition assays. The ability of the tested compounds to inhibit cyclooxygenase inhibition COX-1 and COX-2 were carried out using an enzyme immune assay (EIA) kit (item no. 560131, Cayman Chemical, Ann Arbor, MI, USA) following the manufacturer's instructions according to the previously reported method.[35,36] The concentration that inhibited enzymes by 50% (IC_{50}) was determined. Also, selectivity index (SI) which is defined as (IC_{50} (COX-1)/IC_{50} (COX-2) was calculated and compared with celecoxib.

3.2.2. The *in vitro* anti-inflammatory assay using egg albumin. Protein denaturation method was proposed by Mizushima *et al.*[37] with certain modifications has been utilized to evaluate the anti-inflammatory (*in vitro*) activity (ESI†).

3.3. *In silico* studies

3.3.1. Molecular docking. Molecular modeling studies were carried out using Chimera-UCSF and AutoDock Vina on Linux-based systems. Proteins and the structure of compounds were prepared and optimized using Maestro, then binding sites inside proteins were determined using grid-box dimensions around the co-crystallized ligands. The investigated compounds were docked against the protein structures of COX-1 (PDB = 3KK6)[38] and COX-2 (PDB = 1CVU)[39] using AutoDock Vina software.[40] AutoDock Vina was used for improving protein and ligand structures and to favor them energetically. Binding activities interpreted molecular docking results in terms of binding energy and ligand–receptor interactions. The visualization was then done with Chimera.

3.3.2. Bioinformatics study. ADME pharmacokinetics parameters of the most active compound were calculated using a set of web-based software including "MolSoft", "Molinspiration" and "SwissADME" websites as previously described by ref. 41 and 42.

3.4. Development of niosomal formulation to enhance drug delivery and efficacy

3.4.1. Quantification of the drug using UV spectrophotometry. Spectrophotometric spectrum of the drug was detected in the range of wavelength of 200–400 nm. The maximum absorbance wavelength (λ_{max}) was determined. Spectrophotometric assay method for determination of the drug dipropionate was performed.[43]

An accurately and precisely weighed amount of the drug, 10 mg, was dissolved in 100 mL of ethanol to form a solution of concentration of 100 μg mL^{-1}. Aliquots of the formed solution were withdrawn and diluted properly with ethanol to form a series of solutions ranging in concentration from 2.5–25 μg mL^{-1} of the drug in ethanol. The absorbance of each concentration at λ_{max} was determined and recorded.

Experiment was repeated three times to assure reproducibility of method. Average absorbance was plotted against concentration to construct calibration curve.

The calibration curves of the drug in phosphate buffers of pH 6.8 was constructed following the same method but with replacing ethanol with phosphate buffer of pH 6.8 (BP 2013). This was done to quantify the drug in the *in vitro* release study.[44]

3.4.2. Preparation of plain niosomes. Plain niosomes, PNi, were prepared using thin film-hydration method as reported with slight modification.[45,46] Different components (span 60, span 80, cholesterol, Tween 20 and Tween 80) were used to conduct the preliminary studies so that, the best formula with the best physicochemical characteristics could be obtained (data are not shown). Components, (span 60, cholesterol, and tween 80), in the ration of (120 : 60 : 1 w/w, respectively), were dissolved in 10 mL of chloroform : methanol mixture (1 : 1, v/v) in a round-bottom flask using a BUCHI Rotavapor (Buchi R-215 Advanced Rotavapor with V-Condensor and V-850 Controller). Afterwards, the organic solvents were removed under vacuum in a rotary evaporator at 40 °C for 20 min. To form a thin film; and kept in a desiccator under vacuum for 2 h to ensure total removal of trace solvents. Afterwards, hydration of the film was carried out using 5 mL of distilled water at 55 °C. The niosomal suspension was then sonicated for 15 minutes using a probe sonicator (Fisherbrand™ Model 120, Thermo Fisher Scientific Inc., MA, USA).

The niosomal suspension was left to mature overnight at 4 °C and stored at refrigerator temperature for further studies.

3.4.3. Preparation of drug-loaded niosomes. Drug-loaded niosomes, DNi, were prepared utilizing the same procedure stated for preparing PNi, however, the drug was dissolved with the lipids and surfactants before drying and film formation.

3.4.4. Determination of percentage of yield. Method for determination of percentage of niosomal yield was reported earlier in a previous research paper.[23] Simply, samples, 5 g each, were taken from the prepared niosomes. Samples were then diluted and centrifuged for 45 minutes at 20 000 rpm. The crop of solid residue was collected, left to dry, and weighed (Cubis® II Essentials MCE, Sartorius AG, Göttingen, Germany). Yield percent was calculated using the following formula:

$$\text{Yield percent} = (W_r/W_i) \times 100$$

where, W_r is the total weight of the solid residue, and W_i is the initial weight of excipients utilized in the preparation.

3.4.5. Determination of particle size and particle size distribution. Samples were placed in the hydro S unit of the Malvern® Mastersizer instrument (Mastersizer 2000, vers. 5.54, Wet 2000 S, Malvern Instruments Ltd., Malvern, Worcs, UK). Stirring was utilized to distribute the sample uniformly.

Span value was used for measuring the extent of particle size distribution.

3.4.6. Determination of entrapment efficiency and drug loading. The used method for separating free and entrapped drug in this research was through utilization of centrifuge for its simplicity.[23,47] A volume of 5 mL of DNi sample was diluted to 15 mL with distilled water and then was centrifuged at 15 000 rpm for 2 cycles each spent 60 min. To separate the niosomes from the aqueous phase (HERMLE Labortechnik GmbH, Germany).

The supernatant was then decanted, filtered with 0.2 μm filter, and analyzed by UV-VIS spectroscopy at 334 nm (*cf.* ESI†). The amount of free drug was determined and the percent entrapment efficiency (EE%) of the drug was given by the formula:[48,49]

$$\text{EE\%} = ((W_L - W_F)/W_L) \times 100$$

While the percent drug loading (DL%) was given by the formula:[48,49]

$$\text{DL\%} = ((W_L - W_F)/W_{tN}) \times 100$$

where, EE% is the percent entrapment efficiency, DL% is the percent drug loading, W_L is the amount of drug loaded in formula, W_F is the amount of the free drug determined in the supernatant, and W_{tN} is the weight of drug-loaded nanoparticles.

3.4.7. Determination of thermal behavior of the drug. Thermal behavior of the drug was determined using differential scanning calorimetry (DSC). Structural alterations of materials are usually accompanied by heat exchanges, *e.g.*, uptake of heat during melting or emission of heat during crystallization. DSC is designed to measure these heat exchanges during controlled temperature programs and allows drawing conclusions on the structural properties of a sample.[50–52]

Samples of the pure drug were left to dry completely at room temperature. A samples of 3 mg each was placed in 40 μL aluminum pans and then crimped inside them upon closure of the pans using special piston. Sample-containing pan was then heated up at a rate of 10 °C min^{-1}. Under constant purging of nitrogen gas at a rate equivalent to 30 mL min^{-1} (Shimadzu® DSC-60, Kyoto, Japan). The thermal range used was between 25 °C and 350 °C. A reference of an empty aluminum pan having the same dimensions and quality was used for comparing differences in energy absorption or release by the sample.[50,52] Peaks were then analyzed using Shimadzu® DSC-60 data analysis software.

3.4.8. Determination of any drug-excipient possible physical interactions. DSC was utilized to detect any physical interaction between the drug and excipients of niosomes. The test was done as mentioned earlier, however, samples were composed of the pure drug, PNi, and DNi.[23,51]

3.4.9. Transmission electron microscopy (TEM). Test was performed to detect and image morphological and surface characteristics of DNi formula. A 50 μL of properly diluted sample was dropped on copper grid and left to settle down for 5 minutes. Sample was then stained with 4% phosphotungstic acid and left to dry at ambient temperature. Dry sample was then visualized through electron microscope.[53]

3.4.10. Determination of *in vitro* release profile. The release of the drug from DNi formula was done using dialysis bag.[54,55] Simply, an amount of pure drug and niosomal

formulation equivalent to 5 mg of the drug was put in a pre-wetted dialysis bag and sealed from both sides. The dialysis bag was then placed in a 200 mL beaker containing 100 mL of phosphate buffer, pH 6.8, containing 1% Tween 80 to maintain sink conditions.[23] The beaker was situated on stirrer while maintaining the temperature at 37 ± 0.5 °C for 12 h period. At each time point, 1 mL of the dissolution medium was withdrawn for analysis and replenished by an equal volume of pre-heated new dissolution medium. Samples withdrawn were then analyzed using UV-Vis spectrophotometer as mentioned in the ESI section.†

4. Conclusions

Based on SAR studies of the known selective COX-2 inhibitors, a novel series of 2-benzamido-*N*-phenylthiophene-3-carboxamide derivatives was designed, synthesized and identified as selective COX-2 inhibitors. The inhibitory activity of the novel compounds was evaluated against both COX-1 and COX-2 isoforms. Compound 2-benzamido-5-ethyl-*N*-(4-fluorophenyl) thiophene-3-carboxamide **VIIa** showed selective COX-2 inhibition with IC_{50} 0.29 μM and selectivity index 67.24 comparable to celecoxib with IC_{50} value of 0.42 μM and selectivity index 33.8. Molecular docking studies for the most active compound **VIIa** displayed high binding affinity inside COX-2 active site. The suppression of protein denaturation with respect to albumin was a performed as suggestive indicator for the probable anti-inflammatory efficacy of the novel compounds. Compound **VIIa** showed potent anti-inflammatory activity having 93% inhibition with IC_{50} value 0.54 μM compared to celecoxib with 94% inhibition and IC_{50} value 0.89 μM. Despite being effective, compound **VIIa** as a drug candidate suffered a massive drawback which is its poor aqueous solubility. The drug candidate was incorporated in a niosomal nanocarrier drug delivery system to overcome this limiting characteristic and improve its effectiveness. The prepared nanosystem proved physicochemical suitability as a nano drug delivery system with no incompatibility with the drug candidate. The pattern of release of the drug candidate from the niosomal system proved its efficiency to enhance drug solubility, release pattern, and suggested enhance bioavailability at last. Further work regarding formulating the DNi in an oral fast dissolving films, the *in vivo* efficacy of the drug, safety, pharmacokinetic behavior, and pharmacodynamic characteristics determination will be considered in the future work.

Data availability

Data supporting this study are openly available from the corresponding authors.

Author contributions

Conceptualization, Y. M. A.-A.; P. A. H.; M. E. and M. M. S. methodology, Y. M. A.-A.; P. A. H.; and M. E.; software, Y. M. A.-A.; P. A. H.; and M. E.; investigation, Y. M. A.-A.; P. A. H.; and M. E.; resources, Y. M. A.-A.; P. A. H.; and M. E.; data curation, Y. M. A.-A.; P. A. H.; S. R.; A. B. and M. E.; writing—original draft preparation, Y. M. A.-A.; P. A. H.; and M. E.; writing—review and editing, all; funding acquisition, A. B. All authors have read and agreed to the published version of the manuscript.

Conflicts of interest

The authors declare no conflicts of interest.

Acknowledgements

The authors would like to extend their sincere appreciation to the Researchers Supporting Project (RSP2024R64), King Saud University, Riyadh, Saudi Arabia. Authors acknowledge Dr Mohamed S. Nafie [Department of Chemistry, College of Sciences, University of Sharjah, Sharjah (P. O. 27272), United Arab Emirates (UAE); and Chemistry Department, Faculty of Science, Suez Canal University, Ismailia, (P.O. 41522), Egypt] who conducted *in vitro* COX-1 and COX-2 inhibition assays, egg albumin assay, and a molecular docking study using AutoDock Vina with Chimera.

References

1 R. Korbut and T. J. Guzik, in *Nijkamp and Parnham's Principles of Immunopharmacology*, ed. F. P. Nijkamp and M. J. Parnham, Springer, 2019, pp. 139–163.
2 S. Fiorucci, R. Meli, M. Bucci and G. Cirino, *Biochem. Pharmacol.*, 2001, **62**, 1433–1438.
3 S. Bindu, S. Mazumder and U. Bandyopadhyay, *Biochem. Pharmacol.*, 2020, **180**, 114–147.
4 K. Schrör and M. Voelker, in *NSAIDs and Aspirin*, ed. A. Lanas, Springer, Cham, 2016, pp. 107–122, DOI: **10.1007/978-3-319-33889-7_7**.
5 P. Rao and E. E. Knaus, *J. Pharm. Pharm. Sci.*, 2008, **11**, 81s–110s.
6 P. Świątek, M. Strzelecka, R. Urniaz, K. Gębczak, T. Gębarowski, K. Gąsiorowski and W. Malinka, *Bioorg. Med. Chem.*, 2017, **25**, 316–326.
7 D. L. Simmons, R. M. Botting and T. Hla, *Pharmacol. Rev.*, 2004, **56**, 387–437.
8 L. Dong, A. J. Anderson and M. G. Malkowski, *Biochemistry*, 2019, **58**, 3990–4002.
9 A. A. Mabrouk, M. I. Tadros and W. M. El-Refaie, *J. Drug Delivery Sci. Technol.*, 2021, **61**, 102240–102252.
10 G. Carullo, F. Galligano and F. Aiello, *MedChemComm*, 2017, **8**, 492–500.
11 R. Mayer and K. Gewald, *Angew. Chem., Int. Ed. Engl.*, 1967, **6**, 294–306.
12 R. W. Sabnis, *Sulfur Rep.*, 1994, **16**, 1–17.
13 T. J. Reilly, *J. Chem. Educ.*, 1999, **76**, 1557.
14 V. Theodorou, M. Alagiannis, N. Ntemou, A. Brentas, P. Voulgari, V. Polychronidou, M. Gogou, M. Giannelos and K. Skobridis, *J. Org. Chem.*, 2018, 308–319.
15 M. T. Bogert and H. A. Seil, *J. Am. Chem. Soc.*, 1905, **27**, 1305–1310.

16 I. F. Uchegbu and A. T. Florence, *Adv. Colloid Interface Sci.*, 1995, **58**, 1–55.
17 A. Manosroi, P. Wongtrakul, J. Manosroi, H. Sakai, F. Sugawara, M. Yuasa and M. Abe, *Colloids Surf., B*, 2003, **30**, 129–138.
18 C. Terzano, L. Allegra, F. Alhaique, C. Marianecci and M. Carafa, *Eur. J. Pharm. Biopharm.*, 2005, **59**, 57–62.
19 D. Paolino, R. Muzzalupo, A. Ricciardi, C. Celia, N. Picci and M. Fresta, *Biomed. Microdevices*, 2007, **9**, 421–433.
20 O. Mozgova, M. Blazheyevskiy, L. Kryskiw, T. Kucher, O. Shliusar and V. Moroz, *Chem. Pap.*, 2024, 6585–6591, DOI: 10.1007/s11696-024-03558-4.
21 M. Bakshi and S. Singh, *J. Pharm. Biomed. Anal.*, 2002, **28**, 1011–1040.
22 R. A. Hashad, R. A. H. Ishak, S. Fahmy, S. Mansour and A. S. Geneidi, *Int. J. Biol. Macromol.*, 2016, **86**, 50–58.
23 P. A. Hanna, M. M. Ghorab and S. Gad, *Anti-Inflammatory Anti-Allergy Agents Med. Chem.*, 2019, **18**, 26–44.
24 M. Danaei, M. Dehghankhold, S. Ataei, F. Hasanzadeh Davarani, R. Javanmard, A. Dokhani, S. Khorasani and M. Mozafari, *Pharmaceutics*, 2018, **10**, 57–74.
25 V. Ravalika and A. K. Sailaja, *Nano Biomed. Eng.*, 2017, **9**, 242–248.
26 Z. Sezgin-Bayindir, M. N. Antep and N. Yuksel, *AAPS PharmSciTech*, 2015, **16**, 108–117.
27 K. T. Savjani, A. K. Gajjar and J. K. Savjani, *Int. Scholarly Res. Not.*, 2012, **2012**, 195727–195737.
28 F. J. Tinney, W. A. Cetenko, J. J. Kerbleski, D. T. Connor, R. J. Sorenson and D. J. Herzig, *J. Med. Chem.*, 1981, **24**, 878–882.
29 Z. Szlávik, L. Ondi, M. Csékei, A. Paczal, Z. B. Szabó, G. b. Radics, J. Murray, J. Davidson, I. Chen and B. Davis, *J. Med. Chem.*, 2019, **62**, 6913–6924.
30 L. Ouyang, L. Zhang, J. Liu, L. Fu, D. Yao, Y. Zhao, S. Zhang, G. Wang, G. He and B. Liu, *J. Med. Chem.*, 2017, **60**, 9990–10012.
31 K. Clausen and L. SO, *Nouv. J. Chim.*, 1980, **4**, 43–46.
32 A. M. Zaino, R. C. Dash, S. J. James, N. MacGilvary, A. Crompton, K. S. McPherson, M. Stanzione, D. M. Korzhnev, N. J. Dyson and N. Chatterjee, *Bioorg. Med. Chem.*, 2024, **106**, 117755–117765.
33 N. D. Smith, WO2009/026241A1, 2009.
34 I. Kharizomenova, N. Samsonova, N. Kaplina, M. Kapustina and A. Grinev, *Khim. Geterotsikl. Soedin.*, 1980, 45–46.
35 K. R. A. Abdellatif, W. A. A. Fadaly, Y. A. Mostafa, D. M. Zaher and H. A. Omar, *Bioinorg. Chem.*, 2019, **91**, 103–132.
36 B. Roschek Jr, R. C. Fink, D. Li, M. McMichael, C. M. Tower, R. D. Smith and R. S. Alberte, *J. Med. Food*, 2009, **12**, 615–623.
37 Y. Mizushima and M. Kobayashi, *J. Pharm. Pharmacol.*, 1968, **20**, 169–173.
38 G. Rimon, R. S. Sidhu, D. A. Lauver, J. Y. Lee, N. P. Sharma, C. Yuan, R. A. Frieler, R. C. Trievel, B. R. Lucchesi and W. L. Smith, *Proc. Natl. Acad. Sci. U. S. A.*, 2010, **107**, 28–33.
39 J. R. Kiefer, J. L. Pawlitz, K. T. Moreland, R. A. Stegeman, W. F. Hood, J. K. Gierse, A. M. Stevens, D. C. Goodwin, S. W. Rowlinson and L. J. Marnett, *Nature*, 2000, **405**, 97–101.
40 O. Trott and A. J. Olson, *J. Comput. Chem.*, 2010, **31**, 455–461.
41 A. T. Boraei, E. H. Eltamany, I. A. Ali, S. M. Gebriel and M. S. Nafie, *Bioinorg. Chem.*, 2021, **111**, 104877–104891.
42 B. Steinfeld, J. Scott, G. Vilander, L. Marx, M. Quirk, J. Lindberg, K. Koerner and J. Behav, *Health Serv. Res.*, 2015, **42**, 504–518.
43 Y. P. Pancham, B. Girish and S. S. Sanjay, *J. Pharm. Innov.*, 2020, **9**, 5–8.
44 I. Takeuchi, Y. Taniguchi, Y. Tamura, K. Ochiai and K. Makino, *Colloids Surf., A*, 2018, **537**, 411–417.
45 S. Sangkana, K. Eawsakul, T. Ongtanasup, R. Boonhok, W. Mitsuwan, S. Chimplee, A. K. Paul, S. S. Saravanabhavan, T. Mahboob and M. Nawaz, *Nanoscale Adv.*, 2024, **6**, 1467–1479.
46 Y. Thabet, M. Elsabahy and N. G. Eissa, *Methods*, 2022, **199**, 9–15.
47 J. J. Muso-Cachumba, G. Ruiz-Lara, G. Monteiro and C. d. O. Rangel-Yagui, *Braz. J. Pharm. Sci.*, 2023, **59**, e23365–e23374.
48 T. A. Ahmed, *BMC Pharmacol. Toxicol.*, 2020, **21**, 1–12.
49 P. A. Hanna, H. A. Al-Abbadi, M. A. Hashem, A. E. Mostafa, Y. K. Mahmoud, E. A. Ahmed, I. M. Hegab, I. E. Helal and M. F. Ahmed, *Int. J. Pharm.: X*, 2024, **8**, DOI: 10.1016/j.ijpx.2024.100284.
50 R. B. Guerra, D. A. Gálico, B. B. Holanda and G. Bannach, *J. Therm. Anal. Calorim.*, 2016, **123**, 2523–2530.
51 C. Leyva-Porras, P. Cruz-Alcantar, V. Espinosa-Solís, E. Martínez-Guerra, C. I. Piñón-Balderrama, I. Compean Martínez and M. Z. Saavedra-Leos, *Polymers*, 2019, **12**, 5–26.
52 A. A. Wassel, *Biomed. J.*, 2018, **2**, 1–5.
53 P. Pandey, K. Dua and H. Dureja, *Int. J. Biol. Macromol.*, 2019, **139**, 1304–1316.
54 G. Nerli, S. Robla, M. Bartalesi, C. Luceri, M. D'Ambrosio, N. Csaba and F. Maestrelli, *Carbohydr. Polym. Technol. Appl.*, 2023, **6**, 100332–100341.
55 R. Sirati, A. E. Khajehrahimi, R. Kazempoor, S. Kakoolaki and A. Ghorbanzadeh, *Heliyon*, 2024, **10**, e26486–e26497.